TOMOGRAPHY® RESEARCH ARTICLE

Manganese-Enhanced Magnetic Resonance Imaging for Detection and Characterization of Colorectal Cancers

Liang Wen[1], Xinan Shi[2], Liping He[3], and Dan Han[1]

[1]The First Affiliated Hospital of Kunming Medical University, Kunming, China; [2]Chinese Medicine College of Yun Nan, Kunming, Chinac; and [3]Public Health School of Kunming Medical University, Kunming, China

Corresponding Author:
Dan Han, PhD
The First Affiliated Hospital of Kunming Medical University,
295 Xichang Road, 650000 Kunming, Yunnan Province, China;
E-mail: wlleon007@126.com

Key Words: magnetic resonance imaging, manganese-enhanced, colorectal cancer, detection, characterization

Abbreviations: Manganese-enhanced magnetic resonance imaging (MEMRI), colorectal cancer (CRC), manganese (Mn), gadolinium (Gd), computed tomography (CT), magnetic resonance imaging (MRI), T1-weighted image (T1WI), repetition time (TR), echo time (TE), field of view (FOV), hematoxylin and eosin (H&E), microvessel density (MVD)

ABSTRACT

Here, we investigated the diagnostic performance of manganese (Mn)-enhanced magnetic resonance imaging (MEMRI) in colorectal cancer (CRC). The ability of CRC cell lines SW620 and SW480 to uptake Mn was evaluated and compared with a normal colon cell using MEMRI. Subcutaneous xenografts in nude mice underwent MRI examination at tumor sizes of 5, 10, and 15 mm. Contrast enhancement was compared between gadolinium (Gd)- and Mn-enhanced MRI. SW620 and SW480 cell lines took up more Mn^{2+} than normal cells, resulting in 4.5 and 2 times greater T1 value shortening than normal cell using in vitro MEMRI ($P < .001$). Most xenografts (17/23) enhanced markedly on MEMRI. A heterogeneous enhancement pattern invariably noted whether Mn or Gd agents were administered, but tumors imaged using MEMRI showed a greater degree of enhancement with a larger extent of enhanced area than those imaged using Gd-enhanced MRI. The numbers of markedly Mn-enhanced cases were more in the 5-mm-size tumor group than in 10- or 15-mm-size tumor groups. Overall, MEMRI could enhance CRCs and it showed potential in detecting early small lesions and markedly enhancing tumors that had minimal Gd enhancement.

INTRODUCTION

Colorectal cancer (CRC) is the third most common form of cancer and the fourth most common cause of death globally. Colonoscopy and computed tomography (CT) are used for diagnosis and staging because of the lack of an effective serum biomarker (1, 2). However, misdiagnosis of cancer and difficulties with accurate tumor localization in colonoscopy examination along with the relatively low specificity of CT scans underpin the need for improved imaging approaches for increased sensitivity and specificity. Recently magnetic resonance imaging (MRI) was shown to be superior to CT in defining advanced T-stage CRC and in detecting metastatic lesions <10 mm in the liver (3, 4). However, conventional MRI still relies on morphological changes to make a diagnosis. The contrast medium used in conventional MRI, such as Gd-DTPA, is an extracellular nonspecific contrast agent, and lesion detection depends on tumor vascularity. For small early lesions, particularly those with hypovascularity, the diagnostic accuracy of conventional MRI needs to be improved. By contrast, manganese (Mn)-enhanced MRI (MEMRI) using an Mn^{2+} agent confers its enhancement effect largely to Mn uptake by cells rather than lesion vascularity. Moreover, Mn is a required trace element for maintaining normal metabolic and physiological processes in the human body and thus its toxicity is lower than that of gadolinium (Gd) (5, 6). Presently the application of 2 Mn contrast agents used clinically, CMC-001 and Mn-DPDP, is limited to the detection of liver metastasis (7-9). To provide more accurate clinical staging and prognosis, MEMRI could be an important approach to improve early primary CRC detection. This study used $MnCl_2$ as the contrast agent to perform MRI on CRC cell lines and subcutaneous xenograft tumors in nude mice to investigate the diagnostic efficacy of MEMRI to specifically detect early-stage CRC.

MATERIALS AND METHODS

Cell Lines

Human CRC cell lines SW620 and SW480 along with a normal colon cell line CCD841 CoN were purchased from ATCC (Manassas, VA). Cell lines SW620 (lymph node metastasis) and SW480 (primary tumor) were derived from the same patient. Cell lines were cultured in RPMI 1640 medium containing 10% fetal bovine serum (Invitrogen, Rockville, MD) at 37°C in 5% CO2 and 95% humidified air.

ISSN 2379-1381 http://dx.doi.org/10.18383/j.tom.2018.00008

In Vitro MEMRI of Cells

$MnCl_2$ was dissolved in culture media at 0.1 mM for cancer and normal cell lines during their exponential growth phase to observe Mn uptake by cells. After incubation for 60 min, cells underwent centrifugation at 1000 g for 10 min at 37°C, 5% CO_2. The supernatant was removed and fresh media was added to rinse the cell pellets. Cells were recentrifugated, and cell pellets were rinsed again under the same condition for a final centrifugation. The corresponding cell lines without administration of $MnCl_2$ were also centrifuged the same way and served as controls for these studies. Cell pellets were prepared with a depth of about 10 mm in Corning tubes (1.5 mL) for subsequent image examination.

Images were acquired on a clinical 3.0 T MRI scanner with an 8-channel head coil. The temperature in the scanner bore was 25°C. Both T1-weighted image (T1WI) and T1 map images were acquired in the axial plane. First, a 2D spin echo T1WI (2D SE T1WI) was performed with following parameters: repetition time (TR) = 597.22 milliseconds, echo time (TE) = 12.40 milliseconds, field of view (FOV) = 60 mm, section thickness = 1 mm, section interval = 1 mm, number of acquisitions = 20, matrix = 144 × 144. Further, a 2D inversion recovery turbo spin echo (2D IR TSE) for determination of a T1 map was performed: TR = 3000 milliseconds, TE = 18.5 milliseconds, TI = 50, 100, 250, 500, 750, 1000, 1250, 1500, 2000, 2500 milliseconds. FOV = 60 mm, section thickness = 1 mm, section interval = 1 mm, number of acquisition = 20, matrix = 144 × 144. The data calculation and analyses were conducted using a custom program developed in MATLAB (version 7.0; MathWorks, Natick, MA). Both T1 relaxation times with and without Mn administration were calculated on a pixel-by-pixel basis. Three independent measurements were made, and the average values were recorded. The average T1 value shortening was defined as subtraction of average T1 values in 0 mM and 0.1 mM concentrations. The ROI (region of interest) was manually encircled at the cell pellets section with an area of about 7 × 7 mm^2.

Subcutaneous Xenograft Tumors

Female BALB/c nude mice (average weight, 15 g) were kept under specific pathogen-free conditions with an IVC system and cared for in accordance with the guidelines of Laboratory Animal Ethics Committee. Housing conditions included a light:dark cycle of 12 h, temperature of 15°C–27°C, and humidity between 50%–80%. The cages and food and water were sterilized. All implanted tumor growth assays used 1 × 10^6 cells/0.2 mL of phosphate-buffered saline without mycoplasma contamination injected subcutaneously into the right flank of the mice; the tumor size was monitored daily.

MRI of Xenografts

Nude mice (n = 5–7) were randomly selected to undergo MRI after tumor diameters reached 5, 10, and 15 mm. The aforementioned scanner was used, but it was equipped with small-bore phased array radiofrequency coil. $MnCl_2{\cdot}4H_2O$ (Sigma-Aldrich) was dissolved in distilled water to make a 100 mM solution that was further diluted using saline to 50 mM, which was isotonic. Gd-DTPA (0.5 mol/L, Bayer) was diluted to 50 mM by saline for intravenous injection via the tail vein. Mice that were in the prone position with head first were anesthetized with 1.5% isoflurane. The body temperature of the mice was maintained by an air warming system at ~37°C. The tumor was placed at the center of the coil and MRI acquisition was accomplished in the axial plane. First, 2D turbo spin echo T1WI (2D TSE T1WI) was performed with following parameters: section thickness = 2 mm, section interval = 1 mm, TR = 626.17 milliseconds, TE = 23 milliseconds, FOV = 40 mm, matrix = 320 × 320. Second, T1 maps were obtained using a variable flip angle (VFA) method 3D FS T1 TFE (3D fat saturation T1 turbo field echo) was performed: section thickness = 2 mm; section interval = 1 mm; TR = 6.9 milliseconds; TE = 3.7 milliseconds; FOV = 40 mm; flip angle = 2°, 10°, and 20°; and matrix = 256 × 256 (10, 11). Then an IV bolus injection of 0.05 μmol/g Gd-DTPA was administered and repeated T1WI and T1 maps 3 times. After that, 0.3 μmol/g of 50 mM $MnCl_2$ solution was injected peritoneally, and Mn-enhanced T1WI and T1 maps with the same parameters were performed again 24 h later. Data processing was similar as mentioned above. The entire tumor margin on every section was outlined, and the average T1 relaxation time was recorded.

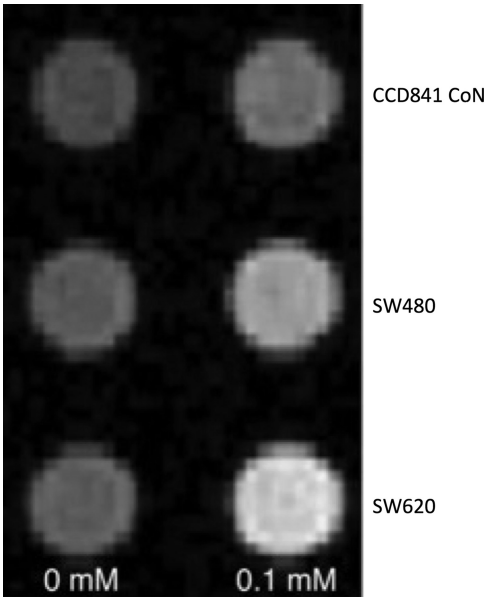

Figure 1. In vitro manganese-enhanced magnetic resonance imaging (MEMRI) of SW620, SW480, and normal cell lines. T1-weighted image (T1WI) of cell pellets from cells exposed to a 0- or 0.1 mM $MnCl_2$ incubated for 60 min revealed both cancer cells and normal cell were enhanced by various degrees; however, cancer cells displayed a more marked level of enhancement versus the normal cellular counterpart.

Histopathology and Immunohistochemistry

Following MRI examination, animals were sacrificed, and the excised tumors were fixed in 10% neutral formalin for pathological study. Hematoxylin and eosin (H&E) staining and microvessel density (MVD) counting of CD34 immunohisto-

Table 1. Comparison of Average T1 Shortening of Cells in In Vitro MEMRI (milliseconds)

Cell Lines	$\bar{x} \pm s$	F	P
SW620	293.13 ± 0.57	2030.259	<.001
SW480	130.10 ± 1.86		
CCD841 CoN	65.02 ± 0.12		

One-way ANOVA was used to compare the differences of average T1 shortening in 3 groups of cells. A significant difference was found between 3 groups ($F = 2030.259$; $P < .001$), and a further paired comparison showed that SW620 cell has the largest T1 shortening, whereas a normal cell has the shortest one.

Table 3. Comparison of T1 Value Shortening Between Mn- and Gd-Enhanced MRI ($\bar{x} \pm s$) (milliseconds)

Tumor Size	Mn-Enhanced	Gd-Enhanced	t	P
5 mm	712.59 ± 38.15	198.87 ± 22.24	40.477	<.001
10 mm	463.68 ± 223.25	257.78 ± 149.95	2.519	.053
15 mm	565.45 ± 183.33	290.36 ± 122.07	3.210	.051

Paired sample t test was used to compare the difference of T1 shortening between two agents in each size group. Significant difference was found in 5 mm-size group ($t = 40.477$, $p < 0.001$).

chemical stained sections were performed. MVD was assessed under a light microscope in the area containing the highest numbers of capillaries and small venules (neovascular "hot spots"). First, the hot spots were identified at low magnification (40×), and then individual microvessels were counted on a 200× field. Any brown-staining endothelial cell or cluster, clearly separate from adjacent microvessels, tumor cells, and other connective tissues, was considered as a single countable microvessel. Vessel lumen exceeding 8 red cells were excluded. The average number of 5 hot spot fields for each case was recorded. The result was reported as average number per 200× field.

Statistical Analysis

SPSS 13.0 was used to perform the analysis. Differences of Mn uptake by cell lines in vitro were compared by using 1-way analysis of variance. Differences in average T1 value shortening induced by Mn^{2+} in xenografts were compared using paired-samples t test. It was not meaningful to perform RxC χ^2 test for comparing the differences in tumor numbers that exhibited marked Mn enhancement between different group sizes owing to limited sample size. A value of $P \leq .05$ was reported as statistically significant.

RESULTS

In Vitro MEMRI of Cells

All 3 cell lines incubated in media containing 0.1 mM $MnCl_2$ exhibited increased Mn uptake as shown on T1WI, evident as an increase in signal intensity as compared with cells without exposure to $MnCl_2$ (Figure 1). Furthermore, T1 map analysis showed that the average T1 shortening in SW620 and SW480 was 4.5 and 2 times more than that in CCD841 CoN, respectively. The 1-way analysis of variance showed significant difference in average T1 shortening between the 3 cell lines ($P < .001$) (Table 1).

MRI of Xenografts

All 23 tumors, including SW620 (n = 5) and SW480 (n = 18), underwent MEMRI, among which 21 were scanned by Gd-enhanced MRI. Two SW480 tumor-bearing mice in the 15-mm-size tumor group failed owing to inadequate tail vein injection of the contrast agent. None of the SW620 tumor-bearing mice survived the tumor size exceeding 5 mm. All tumors displayed slight to moderately higher signal intensity relative to muscle on 2D TSE T1WI. More tumors with marked enhancement were shown on the Mn-enhanced scan than on the Gd-enhanced scan (Table 2) (marked enhancement was defined as average T1 shortening ≥500 milliseconds, the minimal enhancement was defined as average T1 shortening of ≤300 milliseconds). All tumors displayed a heterogeneous enhancement pattern after contrast media administration; however, the enhancement degree and extent were different between 2 contrast agents. The T1 map analysis indicated that the average T1 value shortening of both SW620 and SW480 tumors in the 5-mm-size tumor group was >500 milliseconds on the Mn-enhanced scan, although it was <300 milliseconds on the Gd-enhanced scan. The t test found a significant difference in the enhancement degree between the 2 contrast agents ($P < .001$). However, no significance was found in the 10- or 15-mm-size tumor groups (Table 3). In addition, the extent of the tumor enhancement was larger on Mn-enhanced scans (Figures 2–4).

Table 2. Cases of Tumor With Marked Enhancement in Different Size Groups (Mn/Gd)

	5 mm		10 mm		15 mm	
	Scanned Case	Marked Enhancement Case	Scanned Case	Marked Enhancement Case	Scanned Case	Marked Enhancement Case
SW620	5/5	5/0	0	0	0	0
SW480	5/5	5/0	6/6	3/1	7/5	4/0

Not meaningful to perform the statistical test because of limited sample size.

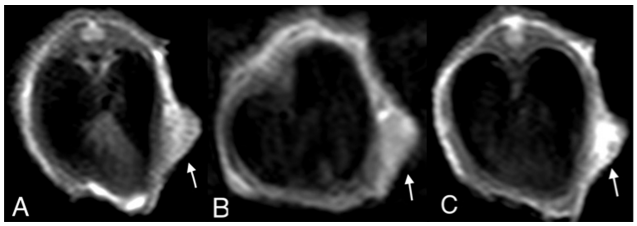

Figure 2. 2D turbo spin echo (2D TSE) T1WI of an SW620 xenograft in the 5-mm tumor group (arrow). In the unenhanced scan, the tumor manifests as a mildly high signal intensity relative to muscle (A). In the conventional gadolinium (Gd)-enhanced scan, the tumor enhances slightly and inhomogeneously (B). In the Mn-enhanced scan, more prominent and a larger extent of enhancement is readily noted (C).

Histopathology and Immunohistochemistry

Routine H&E staining was performed on all tumors, and all sections were diagnosed as moderate-to-low differentiation adenocarcinoma. Under light microscope examination, a similar histological appearance, packed neoplastic cells in patchy distribution with sparse interstitia, and discrete coagulative necrosis were found in all tumors (Figures 5). In total, 21 tumors that underwent Gd-enhanced MRI were further counted for MVD by using CD34 immunohistochemical staining. Sparse neovascularity was shown via MVD results, with a minimum number of 11.4 and a maximum number of 20 per field. The average number and standard deviation was 15.6 ± 2.3.

DISCUSSION

MEMRI has long been used in experimental studies of the central nervous system because Mn^{2+} with 5 unpaired electrons has a strong paramagnetic effect that shortens the longitudinal relaxation time of adjacent water and its analog to Ca^{2+} that is frequently involved in the detection of neural activity (6). More recently, in vivo and in vitro studies regarding MEMRI were reported in choroidal melanoma, head and neck tumor, mesothelioma, breast cancer, and medulloblastoma (5, 12-17). These studies have shown that MEMRI is a promising tool in detection, characterization, and staging of aggressiveness in distinguishing various neoplasms. According to previous reports, the viability of human breast cancer cells was not affected by the supplementation of $MnCl_2$ with concentration up to 1.0 mM (5), and some malignant mesothelioma cells still showed significant Mn uptake even after incubation in $MnCl_2$, with concentration as low as 0.1 mM (14). We decided to use a culture medium at 0.1 mM for our cell incubation studies to achieve as a pronounced enhancement as possible on the one hand and to avoid cell damage on the other. After 60-min incubation under the same conditions, both cancer and normal cells exhibited Mn enhancement on T1WI, with cancer cells showing more enhancement than normal cells. The average T1 value shortening of SW620 and SW480 cells was 4.5 and 2 times greater than normal cell, respectively. Thus in vitro evidence showed that Mn uptake in cancer cells was greater than that in normal cells, based on MEMRI, indicating that this approach could be used to facilitate detection of CRC using MEMRI. To verify this result, xenograft studies using MRI were subsequently performed.

Unenhanced scans of SW620 and SW480 solid tumors exhibited mild-to-moderate high signal intensity relative to muscle. This may be explained by the histopathological results that packed tumor cells with minimal interstitia were found in all tumors. On MEMRI, all 5 SW620 tumors and 12/18 SW480 tumors displayed marked enhancement. This in vivo study further supports the concept that CRCs (17/23) may be detected by MEMRI.

On MEMRI, all 10 xenografts in the 5-mm-size tumor group enhanced markedly, whereas only 7/13 tumors in the 10- and 15-mm-size tumor groups showed marked enhancement. Although it was not meaningful to perform a χ^2 test to compare the difference in case numbers of marked enhancement tumor owing to the limited sample size, this still deserves a note, as in another study of human breast cancer, a similar phenomenon of different sizes was reported (5). Breast cancer xenografts with the smallest volume (≤ 5 mm^3) showed the most prominent Mn enhancement in comparison to those with larger volumes. This could be explained by the possibility that Mn^{2+} accumulation in smaller-sized tumors can easily reach relatively higher concentration levels versus larger-sized tumors, leading to greater T1

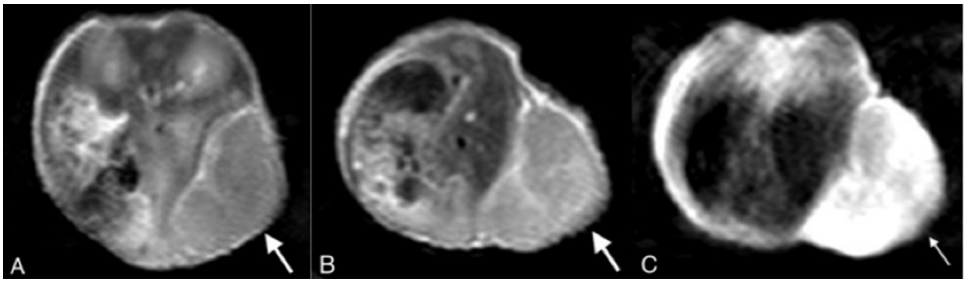

Figure 3. 2D TSE T1WI of an SW480 tumor in the 15-mm-size tumor group (arrow). In the unenhanced scan, the tumor exhibits moderately high signal intensity relative to muscle (A). The conventional Gd-enhanced scan reveals mild enhancement of tumor (B). In the Mn-enhanced scan, the tumor displays marked enhancement along with a larger extent of the enhanced area (C). But both images demonstrate heterogeneous patterns of enhancement.

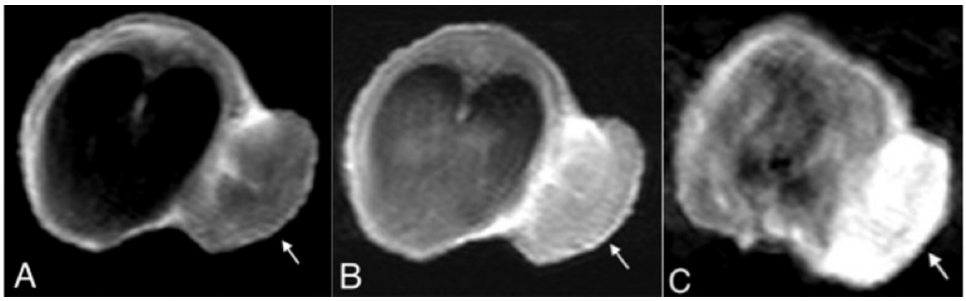

Figure 4. 2D TSE T1WI of an SW480 tumor in the 10-mm-size tumor group (arrow). In the unenhanced scan, the tumor shows slightly elevated signal intensity relative to muscle (A). The conventional Gd-enhanced scan reveals mild enhancement within the tumor (B); In the Mn-enhanced scan, the tumor manifests a marked but heterogeneous enhancement (C).

shortening effect. The findings of these studies indicated that MEMRI has the potential to detect early small cancers, but more studies with larger numbers are needed for confirmation.

Regarding the observed Mn enhancement pattern, the use of it either Mn or Gd agent was inhomogeneous in all tumors. This was different from the observation in a breast cancer study. Alhamami et al. reported that implanted human breast cancers tended to show homogeneous Mn enhancement in contrast to rim enhancement using Gd agents (5). Our finding was more consistent with findings from a malignant mesothelioma study by Hasegawa et al. (14). In that study, most of the mesothelioma xenografts exhibited heterogeneous enhancement both on Mn- and Ga-enhanced MRI. This discrepancy was mainly attributed to differential histological components. In breast cancer studies, both Alhamami et al. and Ganesh T. et al. (5, 17) found that the microvessels were mainly located at the periphery of tumors with packed cells. Whereas in the CRCs of the present study, there were randomly distributed, sparse neovascular components staining in packed tumor cells with discrete necrosis. This corresponded to the inhomogeneous MRI enhancement pattern. However, the enhancement degree between Mn and Ga agents, as well as the extent of the enhanced area, was different. The average T1 value shortening in all 10 tumors in the 5-mm-size tumor group was >500 milliseconds; by comparison, T1 values were <300 milliseconds on Gd-enhanced scans. This difference was statistically significant, although it was not significant in the 10- or 15-mm-size tumor groups. This suggests that MEMRI could markedly enhance tumors that showed minimal enhance-

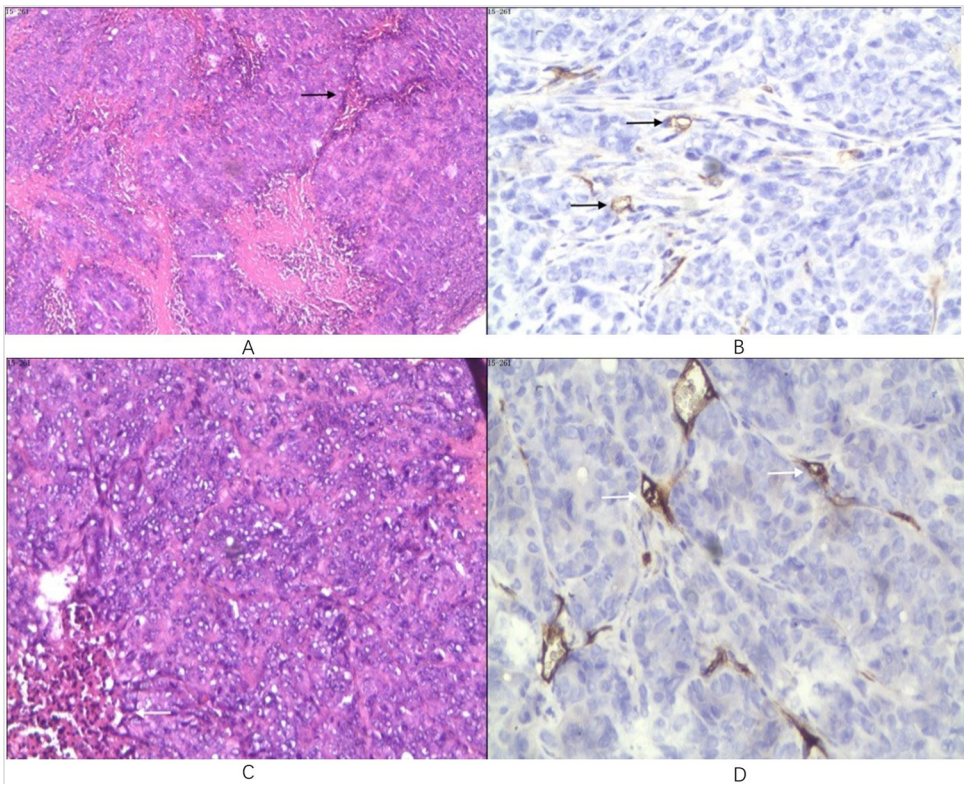

Figure 5. Histopathological photomicrograph of an SW480 tumor in the 10-mm-size tumor group (A and B). Hematoxylin and eosin (H&E) staining 40× (A). Packed tumor cells with few interstitia (black arrow) and discrete coagulative necrosis (white arrow) are shown. CD34 immunohistochemical staining 200× (B). Sparse microvessel staining (arrows) are shown. Histopathological photomicrograph of an SW620 tumor in the 5-mm-size tumor group (C and D). H&E staining 100× (C). Few interstitia (white arrow) within diffuse tumor cells are shown. CD34 immunohistochemical staining 200× (D). Arrows point to sparse microvessels.

ment on conventional Gd-enhanced MRI, particularly the smaller lesions. This was likely because of different enhancing mechanisms of Mn and Ga agents. MEMERI is an intracellular-specific imaging, and its enhancement effect is more dependent on Mn uptake by cells; on the contrary, Gd is an extracellular nonspecific contrast medium and its enhancement effect relies primarily upon tumor vascularity. In the present study, only a few microvessels were found by CD34 staining, which likely resulted in less-conspicuous enhancement in most cases following Gd administration. But because of the dense popularity of tumor cells, even the most hypovascular lesions still enhanced markedly on MEMRI. However, there were 6 tumors in the 10- and 15-mm-size groups that enhanced only minimally (average T1 shortening, $<$300 milliseconds) on MEMRI, indicating that the histopathological change was not the only factor underlying the different enhancing degrees between the 2 agents. Tumor size, agent delivery/volume, and time point of scan may all contribute. This study used intraperitoneal injection to prolong the slow release of Mn^{2+} into the blood stream while avoiding toxicity rather than IV infusion with a uniform dose of 0.3 μmol/g. So the possible explanation for differences would be the scan timing. At 24 h after Mn administration, some tumors might not reach Mn peak uptake or a portion of Mn^{2+} may have already washed out, which makes MEMRI at that time point not truly reflective of optimal tumor Mn enhancement. However additional scans over the 24-h time frame would not be practical owing to the vulnerable physical status of nude mice. Finally, the contribution of extracellular Mn^{2+} retention to tumor enhancement effect should not be overlooked even though very few interstitia were found in our cases (18).

The main limitation in this study was the limited sample size owing to difficult intravenous administration through the small lumen of the tail vein in nude mice and the factor that none of the SW620 tumor-bearing mice survived the tumor size exceeding 5 mm. Also, we did not perform dynamic MEMRI studies, as there was an additional risk of loss of animals because of multiple anesthetization manipulations, which might also result in the missed peak phase of Mn uptake in some less-enhanced tumors by MEMRI.

In summary, both in vitro and in vivo studies indicated that MEMRI not only can enhance CRCs but also holds promise for detection of early-stage lesions and for detection of tumors that have minimal Gd enhancement.

ACKNOWLEDGMENTS

We thank the Institutional Animal Care Committee for granting permission for conducting this study. We also thank the guarantor Dan Han for advice on our study design. The coauthor Dr. Liping He, has contributed with expertise in statistics. This study was funded by Applied Basic Research Project-Union Foundation of Science and Technique Department of Yunnan Province and Kunming Medical University (2017FE467(-048)).

Disclosures: No disclosures to report.

Conflict of Interest: The authors have no conflict of interest to declare.

REFERENCES

1. Brenner H, Kloor M, Pox CP. Colorectal cancer. Lancet. 2014;383:1490–1502.
2. Liu Z, Zhang Y, Niu Y, Li K, Liu X, Chen H, Gao C. A systematic review and meta-analysis of diagnostic and prognostic serum biomarkers of colorectal cancer. PloS One. 2014;9:e103910.
3. Al-Sukhni E, Milot L, Fruitman M, Beyene J, Victor JC, Schmocker S, Brown G, McLeod R, Kennedy E. Diagnostic accuracy of MRI for assessment of T category, lymph node metastases, and circumferential resection margin involvement in patients with rectal cancer: a systematic review and meta-analysis. Ann Surg Oncol. 2012;19:2212–2223.
4. Kaur H, Choi H, You YN, Rauch GM, Jensen CT, Hou P, Chang GJ, Skibber JM, Ernst RD. MR imaging for preoperative evaluation of primary rectal cancer: practical considerations. Radiographics. 2012;32:389–409.
5. Alhamami M, Bayat Mokhtari R, Ganesh T, Tchouala Nofiele J, Yeger H, Margaret Cheng HL. Manganese-enhanced magnetic resonance imaging for early detection and characterization of breast cancers. Mol Imaging. 2014;13.
6. Massaad CA, Pautler RG. Manganese-enhanced magnetic resonance imaging (MEMRI). Methods Mol Biol. 2011;711:145–174.
7. Koh DM, Brown G, Riddell AM, Scurr E, Collins DJ, Allen SD, Chau I, Cunningham D, deSouza NM, Leach MO, Husband JE. Detection of colorectal hepatic metastases using MnDPDP MR imaging and diffusion-weighted imaging (DWI) alone and in combination. Eur Radiol. 2008;18:903–910.
8. Rockall AG, Planche K, Power N, Nowosinska E, Monson JP, Grossman AB, Reznek RH. Detection of neuroendocrine liver metastases with MnDPDP-enhanced MRI. Neuroendocrinology. 2009;89:288–295.
9. Albiin N, Kartalis N, Bergquist A, Sadigh B, Brismar TB. Manganese chloride tetrahydrate (CMC-001) enhanced liver MRI: evaluation of efficacy and safety in healthy volunteers. MAGMA. 2012;25:361–368.
10. Cheng HL, Wright GA. Rapid high-resolution T(1) mapping by variable flip angles: accurate and precise measurements in the presence of radiofrequency field inhomogeneity. Magn Reson Med. 2006;55:566–574.
11. Cheng HL, Stikov N, Ghugre NR, Wright GA. Practical medical applications of quantitative MR relaxometry. J Magn Reson Imaging. 2012;36:805–824.
12. Braun RD, Gradianu M, Vistisen KS, Roberts RL, Berkowitz BA. Manganese-enhanced MRI of human choroidal melanoma xenografts. Invest Ophthalmol Vis Sci. 2007;48:963–967.
13. Seshadri M, Hoy A. Manganese-enhanced MRI of salivary glands and head and neck tumors in living subjects. Magn Reson Med. 2010;64:902–906.
14. Hasegawa S, Koshikawa-Yano M, Saito S, Morokoshi Y, Furukawa T, Aoki I, Saga T. Molecular imaging of mesothelioma by detection of manganese-superoxide dismutase activity using manganese-enhanced magnetic resonance imaging. Int J Cancer. 2011;128:2138–2146.
15. Nofiele JT, Czarnota GJ, Cheng HL. Noninvasive manganese-enhanced magnetic resonance imaging for early detection of breast cancer metastatic potential. Mol Imaging. 2014;13.
16. Suero-Abreu GA, Praveen Raju G, Aristizabal O, Volkova E, Wojcinski A, Houston EJ, Pham D, Szulc KU, Colon D, Joyner AL, Turnbull DH. In vivo Mn-enhanced MRI for early tumor detection and growth rate analysis in a mouse medulloblastoma model. Neoplasia. 2014;16:993–1006.
17. Ganesh T, Mokhtari RB, Alhamami M, Yeger H, Cheng HL. Manganese-enhanced MRI of minimally gadolinium-enhancing breast tumors. J Magn Reson Imaging. 2015;41:806–813.
18. Gianolio E, Arena F, Di Gregorio E, Pagliarin R, Delbianco M, Baio G, Aime S. MEMRI and tumors: a method for the evaluation of the contribution of Mn(II) ions in the extracellular compartment. NMR Biomed. 2015;28:1104–1110.